ARKIV

Texture analysis of sandstone surfaces

Norsk Regnesentral
ANVENDT DATAFORSKNING
Norwegian Computing Center/Applied Research and Development

NOTAT/NOTE

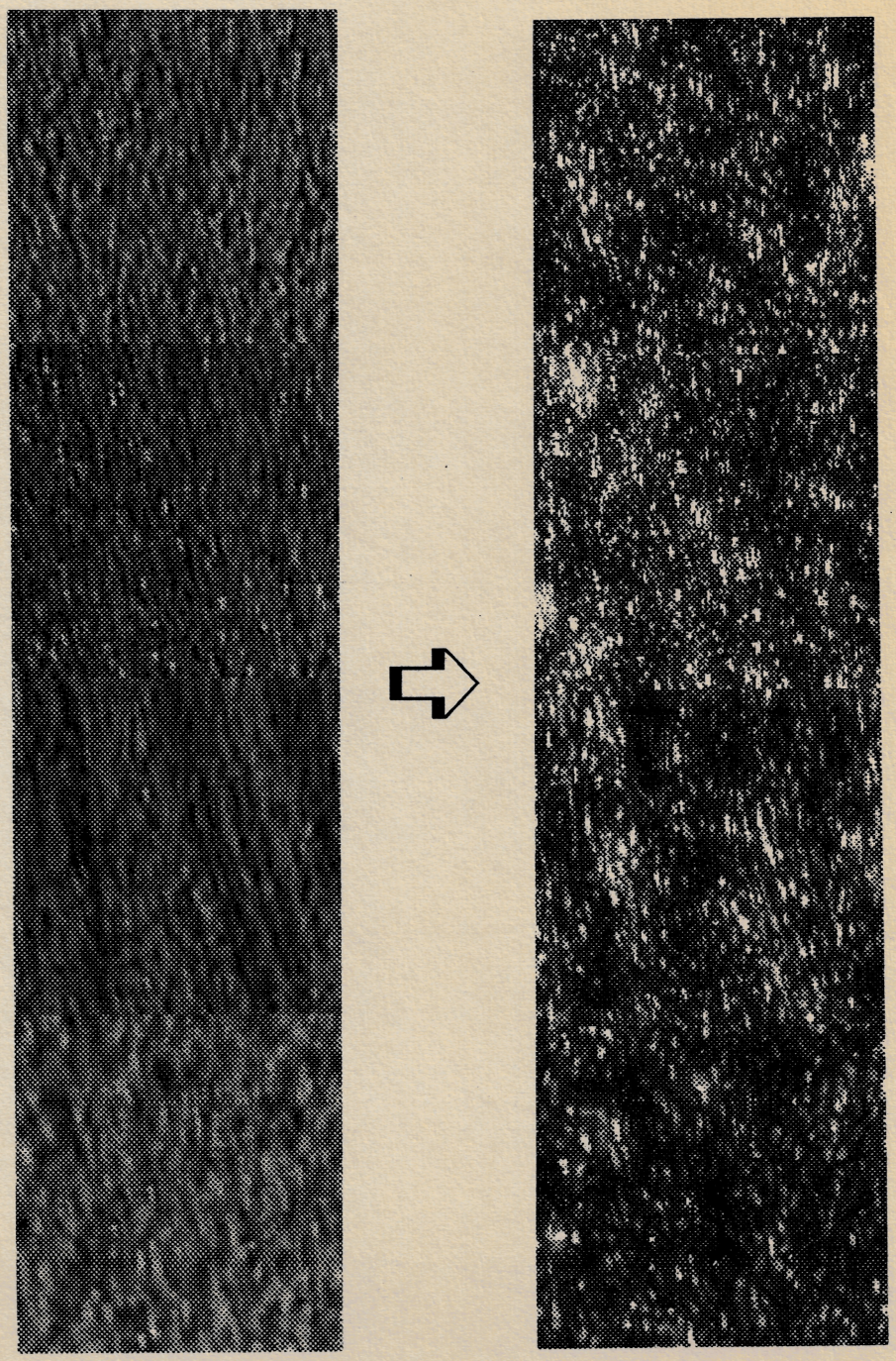

BILD/08/94

Hans Koren
Anne H. S. Solberg
Ole M. Halck
Rune Solberg

Oslo
August 1994

Norsk Regnesentral
ANVENDT DATAFORSKNING

NR-notat/NR-Note

Tittel/Title:
Texture analysis of sandstone surfaces

Dato/Date: August
År/Year: 1994
Notat nr:
Note no:BILD/08/94

Forfatter/Author:
Hans Koren, Anne H.S. Solberg, Ole M. Halck, and Rune Solberg

Sammendrag/Abstract:
This report is the contribution from the Norwegian Computing Center (NR) to the workshop Flat Image Texture Analysis, August 29, 1994, organized by SINTEF. The objective of the workshop was to study possible textural features that can be applied to discriminate between different sandstone facies. Due to limited resources, only relevant textural operators currently available at NR were tested. These are GLCM features, Simultaneous Autoregressive (SAR) models, Gabor filters, and a set of six miscellaneous local texture operators. The available data set consisted of four samples only, so we have been cautious in drawing any final conclusions. The experiments indicate some relationships between the given sandstone characteristics and (1) the gray-level value in the different spectral bands and (2) some of the textural features. Of the four sandstone facies parameters grain size, porosity, and contents of quartz and feldspar, we found indications of relationships between porosity and contents of quartz and some of the textural features. A relatively high correlation was found between gray level and the textural features GLCM Correlation, SAR textural features, Contrast and Homogeneity. Other textural features seem to have some discriminative properties, but at least they cannot be used separately. Before work on further adaptation or development of textural operators is initiated, we strongly recommend that these texture features are tested statistically on a data set consisting of a few hundred samples.

Emneord:

Indexing terms:
Sandstone surfaces, texture analysis.
Målgruppe/Target group:

Tilgjengelighet/Availability:
Open
Prosjektdata/Project data:

Prosjektnr/Project no:

Antall sider/No of pages: 36

Satningsfelt:

Research field:

Norsk Regnesentral/Norwegian Computing Center
Gaustadalléen 23, Postboks 114 Blindern, N-0314 Oslo, Norway
Telefon 22 85 25 00, telefax 22 69 76 60

Contents

1 Introduction

This report is the contribution from the Norwegian Computing Center (NR) to the workshop *Flat Image Texture Analysis*, August 29, 1994, organized by SINTEF. The objective of the workshop is to study possible textural features that can be applied to discriminate between different sandstone facies. If such methods exist or can be developed by the contributors of the workshop, the best methods will be evaluated by Reslab A/S and Norsk Hydro A/S for implementation in a sandstone characterization system.

Sandstone analysis at Reslab A/S is currently done by manual inspection of digitized video images. An image is displayed on a computer screen and analysed by an operator. The operator can do some image enhancement to assist the image interpretation. If some of the interesting parameters can be determined from the texture, and/or determined spectraly from three bands in green, red, and near infrared, sandstone facies characterization could be done partially automatic.

The workshop participants received in advance (1.5 months before the workshop) a data set consisting of two images and a manually determined parameter characterization set. Each image is a mosaic of 12 subimages where each subimage represents a subsection of a sandstone facies (see Figure 1). Each row of subimages consists of the same sandstone sample with three different illumination angles. Hence, there are four different samples in each image. The difference between the two main images is that one has direct, oblique illumination only, and the other has additional diffuse illumination. Each image is composed of the three spectral bands mentioned.

The parameters given for the sandstone facies are values for *grain size*, *porosity*, and *quartz* and *feldspar* content. Grain size and porosity are given as average values for the facies, and the quartz and feldspar contents are given in volumetric percentage determined by microscopic inspection of a thin section of each facies.

With the limited time and financial resources available for the study, we decided only to test textural operators available at NR, except a Gabor filter bank. If none of these textures were satisfactory, it was the hope that the results at least could indicate what type of textural feature which should be developed further.

We initiated the study with a literature search on sandstone characterization based on texture. However, very few publications were found. One of the publications is Haralick et al.'s famous paper [5] where they propose a set of textural features derived from a so-called Gray Level Coocurrence Matrix (GLCM). One of the experiments they carried out was classification of images of sandstone facies. They had a quite large test data set available with 243 sample images, and they achieved promising results with 89% overall correct classification. It has been difficult to compare their experiment with our experiment since we had only four samples, however, we got some of the best results for same features as Haralick et al. found best in their experiment.

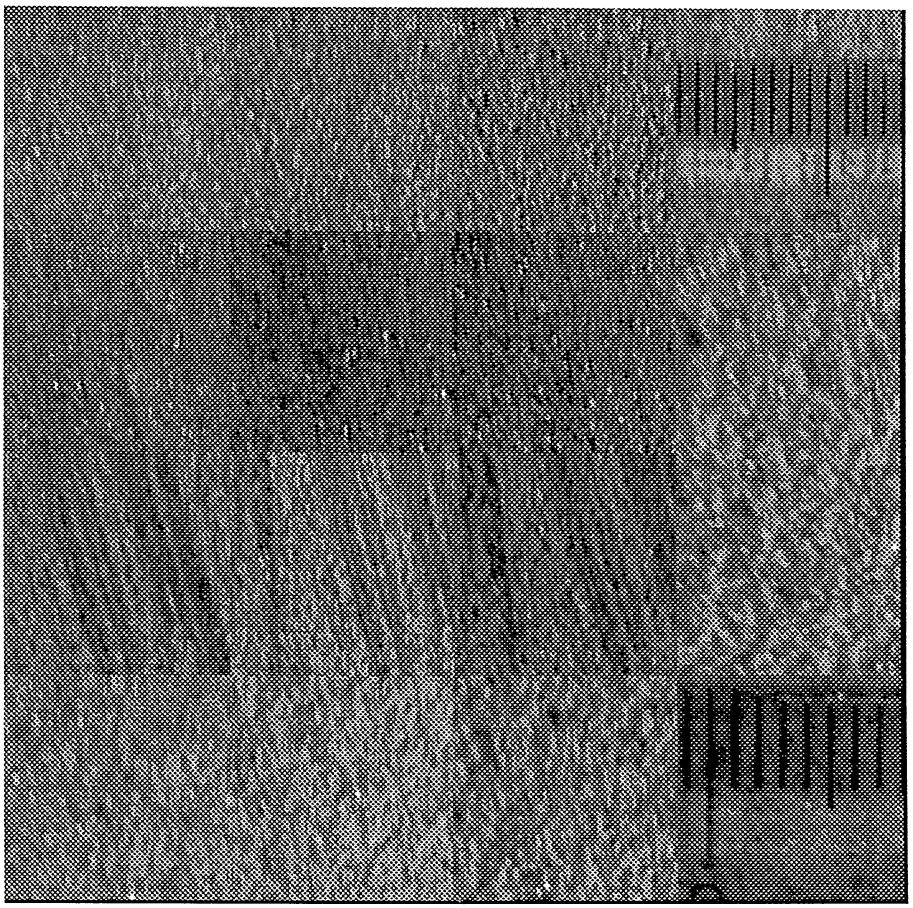

Figure 1: *Original image of sandstone facies without diffuse illumination (near-infrared band).*

2 Textural features tested

The textural features tested are described briefly in this section. More detailed descriptions can be found in the references given here.

2.1 GLCM textural features

The textural features are derived from the so-called Gray Level Coocurrence Matrix (GLCM). The generation of a GLCM is thoroughly described in [5]. The matrix P is a $n \times n$ matrix, where n is the number of gray levels in the image. A matrix element $P(i,j)$ is given by the relative frequency of a pixel pair with gray levels i and j, respectively, at a distance of d pixels, and at an angular direction θ. Typical values of θ are 0, 45, 90 and 135 degrees. In [5] and our work, only nearest neighbour pixels have been considered (i.e. $d = 1$).

A GLCM may be calculated for the whole image, or in a repetitive manner for a moving window in the image. In the first case, the result will be a single textural feature value, and in the other case the result will be a new image where each pixel represents the local texture. In our experiments, we have generated textural images. This has been valuable for visual evaluation, e.g. In some cases, we have derived the mean textural value from the texture image to make quantitative comparisons.

If the image has anisotropic properties, the value of the textural features may be strongly direction dependent. In an image with nearly isotropic properties, the calculated feature values will not differ much with direction. To make the feature values rotation invariant, the mean of the feature values for the four directions may be a valuable textural measure. We used the mean value in our experiments.

Haralick et al. [5] have proposed a set of 14 textural features that can be derived from a GLCM. Some other features have been proposed by Conners et al. [3]. GLCM-based textural operators which were available for our experiment is described briefly in the following. Features $f_1 \ldots f_9$ are from Haralick et al. and features $f_{10} \ldots f_{12}$ are from Conners et al.

Angular Second Moment (ASM)

$$f_1 = \sum_i \sum_j \{p(i,j)\}^2 \tag{1}$$

ASM is a measure of homogeneity. In a homogeneous image, there will be only a few, dominant gray-tone transitions. The matrix will have a few but significant entries. This gives a high value of the squared sum.

Contrast

$$f_2 = \sum_{n=0}^{N_{g-1}} n^2 \left\{ \sum_{i=1}^{N_g} \sum_{j=1}^{N_g} \{p(i,j)\} \right\}, \tag{2}$$

where $|i-j| = n$, and $N-g$ is the number of gray levels in the image. Contrast favours GLCM entries that are not on the diagonal, i.e. entries that represent pixel pairs of different gray-level values.

Correlation

$$f_3 = \frac{\sum_i \sum_j (ij) p(i,j) - \mu_x \mu_y}{\sigma_x \sigma_y}, \tag{3}$$

where μ_x and μ_y are the mean values, and σ_x and σ_y are the standard deviations of p_x and p_y. The correlation feature is a measure of gray-tone linear dependencies in the image.

Variance

$$f_4 = \sum_i \sum_j (i-\mu)^2 p(i,j) \tag{4}$$

Variance favours entries that deviate much from the mean value, and is therefore a measure of variation.

Inverse Difference Moment (IDM)

$$f_5 = \sum_i \sum_j \frac{1}{1+(i-j)^2} p(i,j) \tag{5}$$

IDM is also influenced by the homogeneity in the image. A homogeneous scene gives a high IDM value, while an inhomogenous image gives a GLCM with significant values on non-diagonal entries.

Entropy

$$f_9 = -\sum_i \sum_j p(i,j) \log(p(i,j)) \tag{6}$$

A complex (inhomogenous) scene will have higher values for entropy than more simple scenes. This feature shows similar (but inverse) properties as Angular Second Moment.

Inertia

$$f_{10} = \sum_i \sum_j (i-j)^2 p(i,j) \tag{7}$$

Inertia favours pixel values that deviate much from each other, and is therefore a measure of strong variations.

Cluster Shade

$$f_{11} = \sum_i \sum_j (i+j-\mu_i-\mu_j)^3 p(i,j) \tag{8}$$

Cluster Shade and Cluster Prominence (below) are believed to be measures of the perceptual concepts of uniformity and proximity.

Cluster Prominence

$$f_{12} = \sum_i \sum_j (i+j-\mu_i-\mu_j)^4 p(i,j) \tag{9}$$

2.2 Texture from region statistics

From the texture feature images corresponding to the contrast measure from local statistics [9], we have derived some texture measures from region statistics. The contrast image in Figure 35 has been thresholded. This thresholded image contains a large number of small, bright regions, and the size of these regions appears to be different for different core samples. To investigate this, we have performed a region analysis of the regions. The area of each region is computed, and the mean area size and its standard deviation is computed for each of the different core samples.

2.3 The SAR model textural features

Texture can be modelled by the use of a simultaneous autoregressive (SAR) model [2, 4, 7]. Let the observed image X be represented by a white-noise driven additive system. Assume further that X follows a Gaussian autoregressive (AR) model

$$X(i,j) = \sum_{\{k,l\} \in \mathcal{G}_{ij}} \theta_{kl}(X(i+k, j+l) - \mu_x) + u(i,j), \tag{10}$$

where $\mathcal{G}_{ij}$ is the local neighborhood, μ_x is the mean value for the random process X, and $u(i,j)$ is uncorrelated white noise with variance σ^2 [4]. The least squares estimates of the parameters θ_{kl}, σ^2, and μ_x were used as feature vectors. With a neighborhood consisting

of pixels $(k,l) = ((i-1,j),(i-1,j-1),(i,j-1))$, three θ_{kl} parameters are used. This gives a total of five texture parameters. A window size of 32×32 pixels are used.

2.4 Gabor filters

Gabor filters represent a multi-channel filtering technique which is inspired by the theory for visual information processing in the early stages of human visual system. The channels are characterized by a bank of Gabor filters that nearly uniformly covers the spatial-frequency domain. Filter selection is based on reconstruction of the input image from the filtered images. Textural features are obtained by subjecting each selected filtered image to a nonlinear transformation and computing a measure of "energy" in a window around each pixel. A clustering algorithm can then be used to integrate the feature images and produce a segmentation. A brief description of the filtering is given here. For a complete treatment, see [6] and the references therein.

Either a real even-symmetric or a complex Gabor filter can be specified. The modulation transfer function (MTF) (Fourier-domain description) of an even-symmetric filter has the following "canonical" form.

$$H(u,v) = \exp^{-0.5[\frac{(u-u0)^2}{\sigma_u^2}+\frac{v^2}{\sigma_v^2}]} + \exp^{-0.5[\frac{(u+u0)^2}{\sigma_u^2}+\frac{v^2}{\sigma_v^2}]} \tag{11}$$

These filters have zero degree orientations. Filters with arbitrary orientations are obtained via a rigid rotation.

After computation of the filtered images, each of them is subjected to a nonlinear transformation. Specifically, the following bounded nonlinearity is used:

$$\psi(t) = \tanh(\alpha t)\frac{1-e^{-2\alpha t}}{1+e^{-2\alpha t}}, \tag{12}$$

where α is a constant. This nonlinearity bears certain similarities to the sigmoidal activation function used in artificial neural networks. $\alpha = 0.25$ is used in our experiments. The nonlinearity function has the effect of a "blob detector". The individual blobs are not identified, instead we compute the average absolute deviation from the mean in small overlapping windows. This gives a texture measure which can be interpreted as texture energy.

2.5 Texture measures computed from local statistics

- Power-to-mean ratio, $PMR = \sigma/\mu$, where σ is the local standard deviation and μ is the local mean.

- Skewness, $SKW = \frac{E[(I-\mu)^3]}{\sigma^3}$, where I is the intensity, and $E[]$ denotes expectation.
- Curtosis, $KUR = \frac{E[(I-\mu)^4}{\sigma^4}$
- Contrast, $CONT = 1/(W-1)\sum_{k=1}^{W}[(I(j)-I(k))/\mu]^2$, where W is the number of pixels in a local window around the pixel of interest, j.
- Homogeneity, $HOM = 1/(W-1)\sum_{k=1}^{W}\frac{1}{1+[(I(j)-I(k))/\mu]^2}$
- LIT-SNN, a texture operator which combines the *Symmetric Nearest Neighbor (SNN)* with a *Local Information Transform (LIT)* [1]. This operator counts the number of pixels in a local SNN neighborhood having approximately the same intensity value as the pixel of interest.

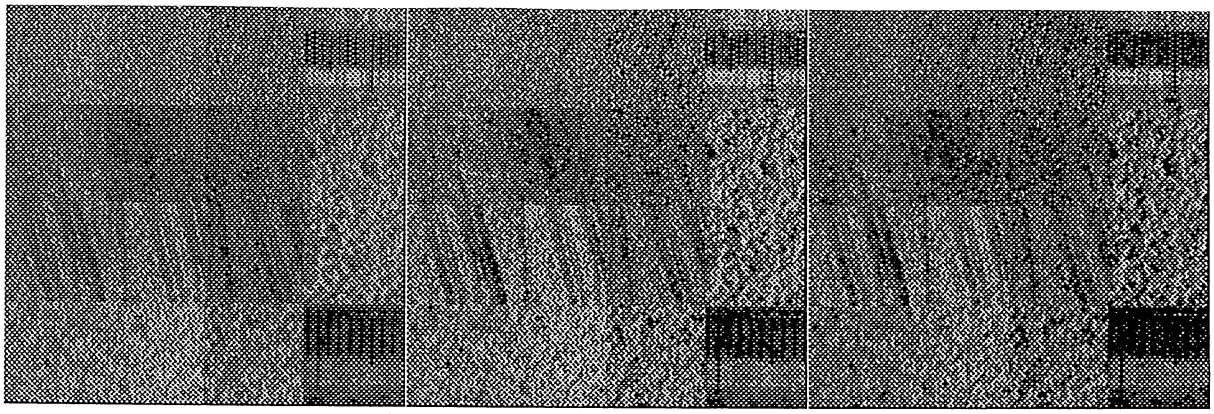

Figure 2: *Image with oblique illumination only. Near-infrared, red, and green bands are shown from left to right.*

3 Experimental results

3.1 The data set

The test data set consists of two images with four different samples of sandstone. The samples are the same in the two images. Each sample has been recorded with a video camera with three different illumination incident angles 45° (high, H), 30° (medium, M), and 15° (low, L). The first image is composed of video subimages with this oblique illumination only, and the second image is with additional diffuse illumination. Each image is composed of three bands where near-infrared (NIR) (1), red (2), and green (3) filters have been applied (the numbers in parenthesis correspond to the band numbers we will use in the following sections).

Figure 2 shows the test image without diffuse illumination. The mosaic is composed of 16 different subimages. One row corresponds to one sample with the illumination situations H, M, and, L, from left to right. (The far right column is of no interest to this experiment.) The four rows, corresponding to the four sandstone facies, will be referred to as sample no. $1, \ldots, 4$, from top to bottom.

The test image *with* additional diffuse illumination is shown in Figure 3. Visually, the two images appear very similar, however, it can be seen that the texture is not quite as sharp in the image with additional diffuse illumination (as could be expected).

Samples 1, 2, and 4 seem to have nearly isotropic surfaces, while sample 3 has marked linear structures across the surface. In addition, for the high (H) illumination situation, a different part of the sample has been recorded than for medium and low illumination. This may complicate the evaluation of the influence of the illumination on this sample.

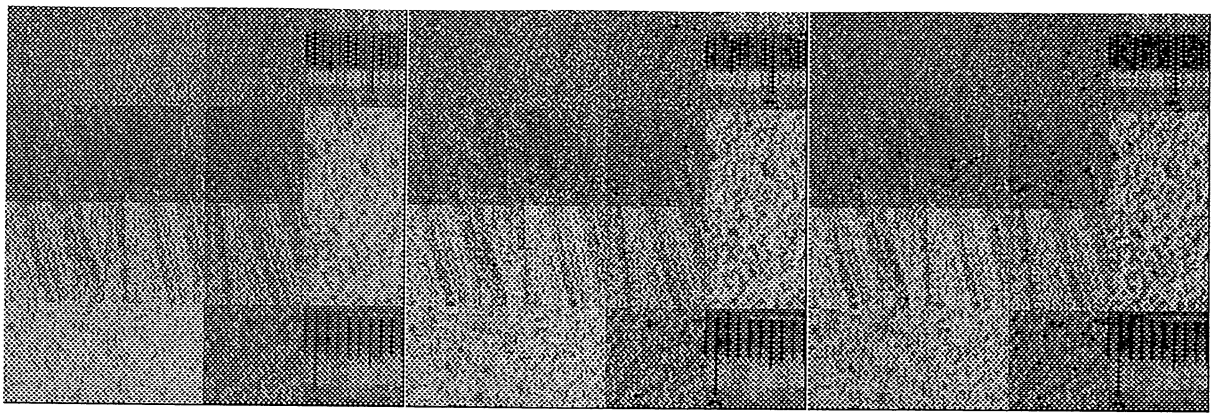

Figure 3: *Image with oblique and diffuse illumination. Near-infrared, red, and green bands are shown from left to right.*

3.2 Experimental procedure

To determine if the sandstone properties for each of the samples in the image mosaic (grain size, porosity, and the contents of quartz and feldspar) may be derived from textural features, the mean feature value has been calculated for each subimage. Border effects from each subimage of size 128 × 128 in the mosaic have been avoided by extracting an image of size 96 × 96 from each of the subimages by using region-of-interest masks.

For each feature image produced, the pixel values have been scaled so that they fill the interval from $[0, \ldots, 255]$. This gave images suitable for visual inspection.

The mean and standard deviation were calculated from the scaled images. Hence, one should avoid to compare the calculated feature values between different features directly. Also, the absolute values of mean and standard deviation should not be used to compare different features. The subimages of one feature corresponding to the four different sandstone samples can, however, be compared directly.

3.3 Multispectral gray-level features

The recorded, multispectral image of one sample may directly tell something about the properties of the sample. We have, therefore, calculated the mean and standard deviation of the gray levels for each sample in the original images. These values have been used to determine if the multispectral gray-level features directly reflect the desired properties: grain size, porosity, and fraction of quartz and feldspar. The values also tell something about the effect of changing illumination and frequency band.

The Figures 4 to 7 show the mean gray level values for all samples, all illuminations and all bands. Each figure show the gray level for one band and one set of illuminations (with or without additional diffuse illumination). The samples are numbered from 1 to 4 from

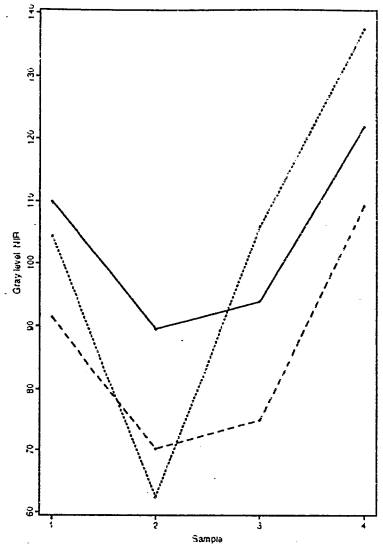

Figure 4: *Gray levels of samples, NIR band.*

the top of the input images. The gray levels for one direction of illumination are connected with a line: High angle, solid line; medium angle, dotted line; and low angle, dashed line.

From these figures, the following can be said about the effects of illumination and frequency band:

- *The angle of illumination influences in different ways the different samples.*

  Without additional illumination, the gray-level values are ordered H, M, L for sample 1. For sample 2 the ordering is H, L, M, and for sample 3 and 4 the gray level values are ordered M, L, H in all cases.

- *Additional diffuse light influences the effect of illumination angle for one sample.*

  The relative values of the gray levels according to illumination angle for sample 1 in the NIR band are ordered H, M, L without, and M, H, L with additional diffuse light. The ordering is also changed for sample 2.

- *Additional diffuse illumination has some influence on the relative gray-level values between different samples.*

  With illumination L the gray level of sample 4 is lower than for sample 3, while without additional diffuse illumination sample 4 has a higher level in all bands. For illumination H, the order is 4, 1, 2, 3 for band NIR and 4, 1, 3, 2 for red and green without additional diffuse illumination. With additional diffuse illumination the order is 4, 3, 1, 2 for all bands.

- *The relative gray level of the samples does not vary much with the frequency band.*

  With NIR, illumination H, and no additional diffuse illumination, the gray-level value of sample 3 is lower than for sample 2, while it is higher in the other bands. In all

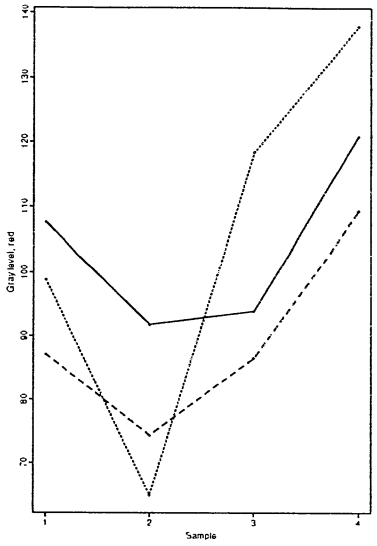

Figure 5: *Gray levels of samples, red band.*

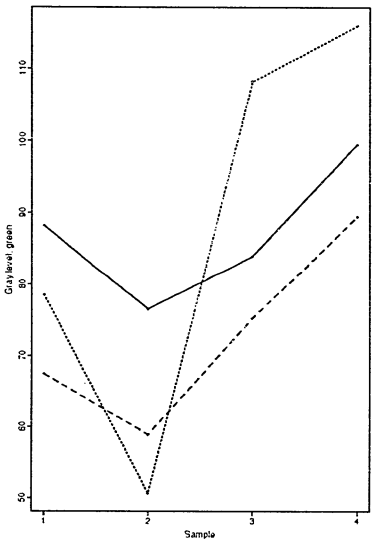

Figure 6: *Gray levels of samples, green band.*

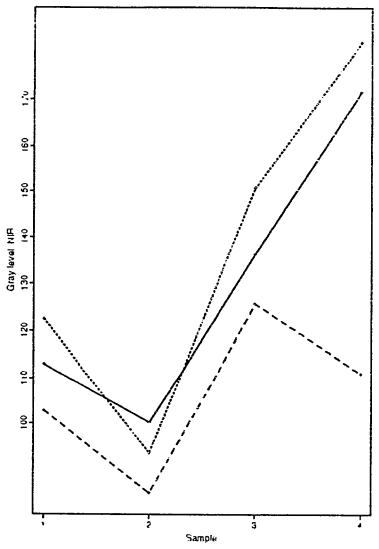

Figure 7: *Gray levels of samples, NIR band. Additional illumination.*

other cases the ordering of the samples according to gray level value do not change with the band.

To see if there is some relation between the mean gray level and the properties of interest, these figures are compared to Figures 8, 9, and 10.

We find that the gray level in some cases reflects the value of porosity and fraction of quartz. The value of these two parameters are ordered 2, 3, 1, 4. The same order of gray level values are found in all the bands with no additional diffuse illumination. In the NIR with illumination L, in the red band with illuminations H and L, and in the green band with illumination H.

3.4 GLCM textural features

All the GLCM textural features described in Section 2 have been computed and inspected visually. The promising and a couple of representatives for the non-promising features are presented here. These include the four features applied by Haralick et al. [5] in their sandstone experiment.

The number of gray levels of the original image (up to 256) are reduced to 16. The GLCM will then be a matrix of size 16×16. This reduces the computation time to a reasonable level. The window size has been chosen to 15×15, so a GLCM is calculated for each pixel in the image within this window. The distance d has been set to 1.

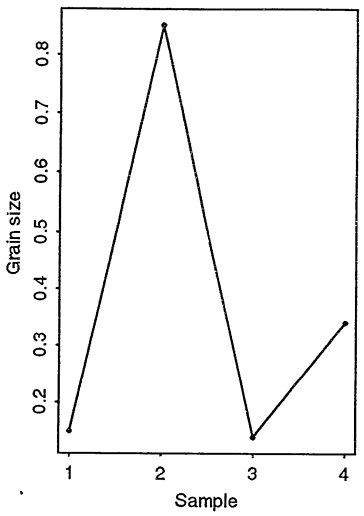

Figure 8: *Grain size of sandstone samples.*

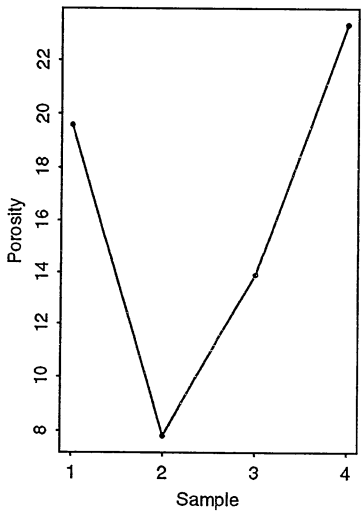

Figure 9: *Porosity of sandstone samples.*

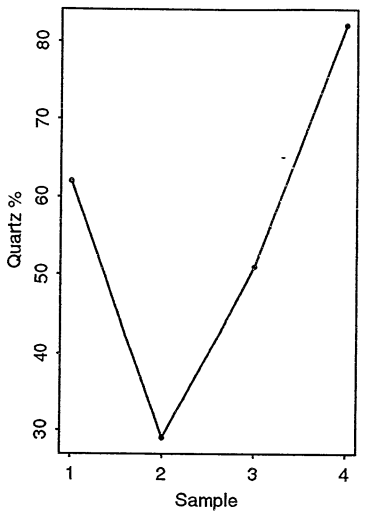

Figure 10: *% quartz of sandstone samples.*

3.4.1 Feature images

Feature images from a number of the textural operators are shown in Figures 11 to 20. When not mentioned, the illumination is without additional diffuse light. Visual inspection has been done to determine if the features somehow reflect the interesting properties of the sandstone samples. For selected features, mean values have been calculated and the relative values have been compared to the sandstone property values. These calculations have mostly been executed for the NIR band with no additional diffuse illumination. For one of the most interesting features, correlation, images are included to show the effects of changing the frequency bands and adding diffuse illumination.

Figure 11: *ASM feature (GLCM). NIR.*

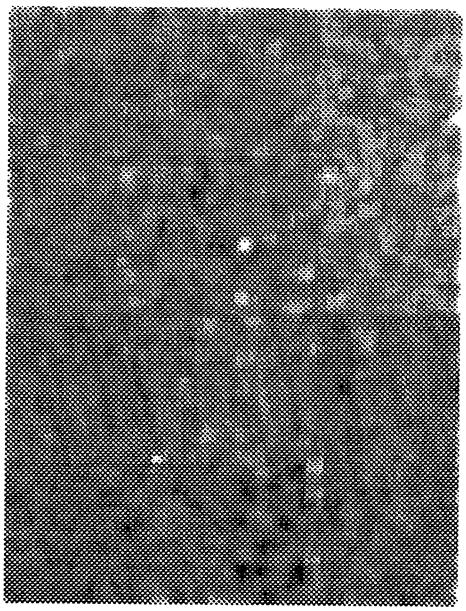

Figure 12: *Contrast feature (GLCM). NIR.*

Figure 13: *IDM feature (GLCM). NIR.*

The effects of using different frequency bands and additional illumination on a textural feature are demonstrated in Figure 21. The image is composed of 6 feature images of the type demonstrated above. The left column shows direct illumination only and the right column shows additional diffuse illumination. The upper row represents the near infrared band, the next row red, and the lower row the green band.

We see that the change of frequency as well as addition of diffuse illumination affect the correlation feature. The effect is different for the different samples. The most prominent difference is seen for the low-angle illumination when adding diffuse illumination, and especially for sample 4.

3.4.2 Mean-value calculations

For some of the most interesting features mean values have been calculated. The results are presented in Figures 22 to 25. The mean feature values are plotted for each sample. Values with corresponding illumination angle are connected with a line: high angle, solid line; medium angle, dotted line; and low angle, dashed line. From these figures we can see the following: For a single feature, the ordering of mean values for the four samples changes with the illumination. And the influence of illumination changes from feature to feature.

For the contrast feature (see Figure 22), the mean values decrease from sample 1 through 4 for all illumination angles. There is one exception for the medium angle, where the mean value is higher for sample 3 than for sample 2. The contrast feature does not seem to reflect the desired property values for the given samples.

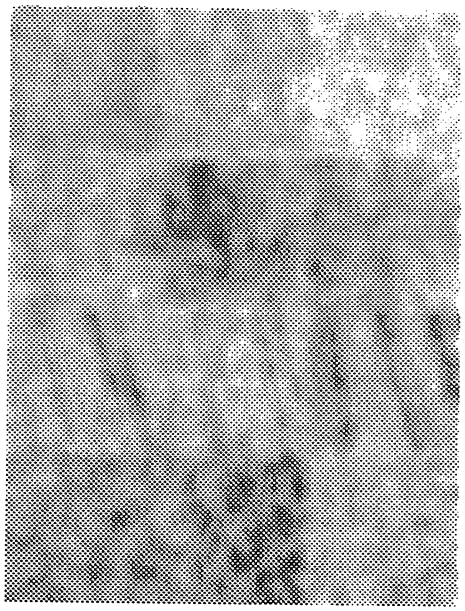

Figure 14: *Entropy feature (GLCM). NIR.*

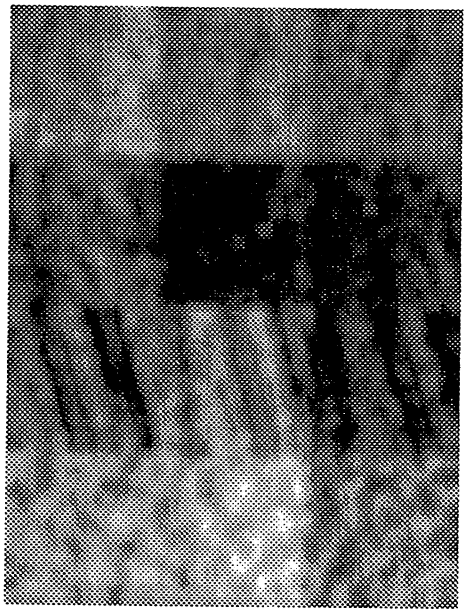

Figure 15: *Correlation feature (GLCM). NIR.*

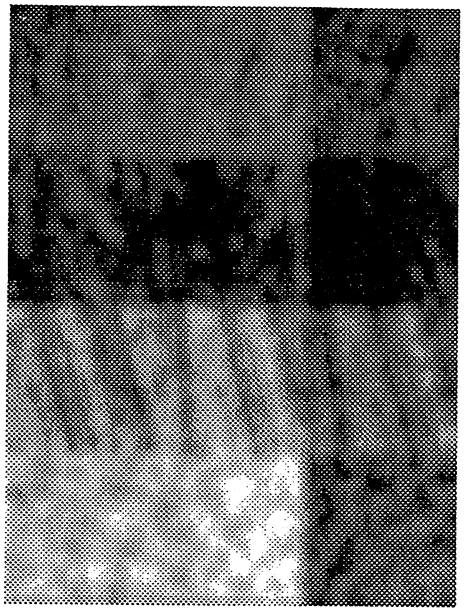

Figure 16: *Correlation feature (GLCM). NIR. With additional diffuse illumination.*

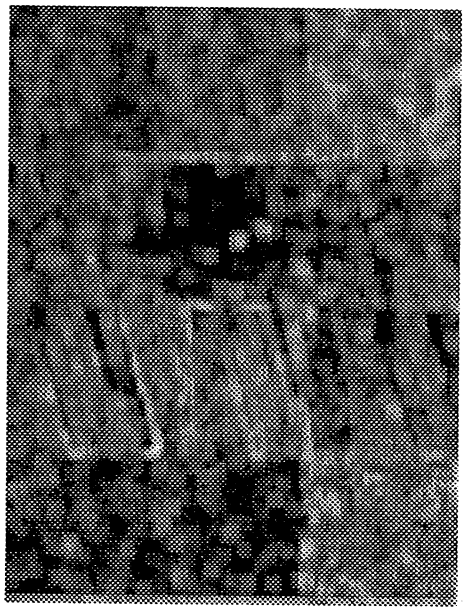

Figure 17: *Variance feature (GLCM). NIR.*

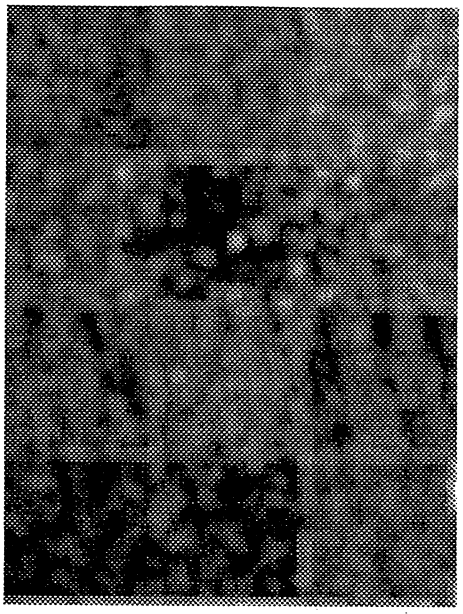

Figure 18: *Inertia feature (GLCM). NIR.*

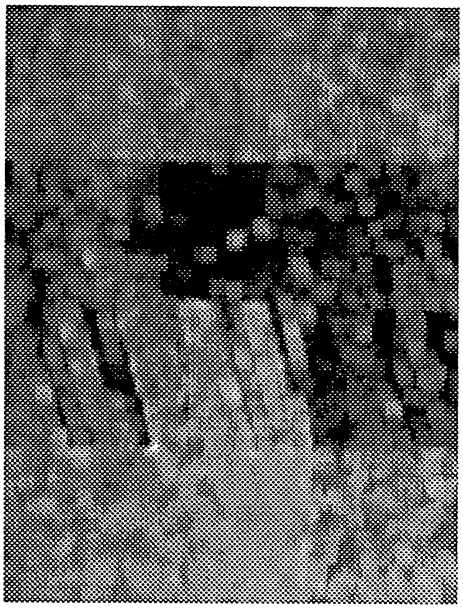

Figure 19: *Cluster shade feature (GLCM). NIR.*

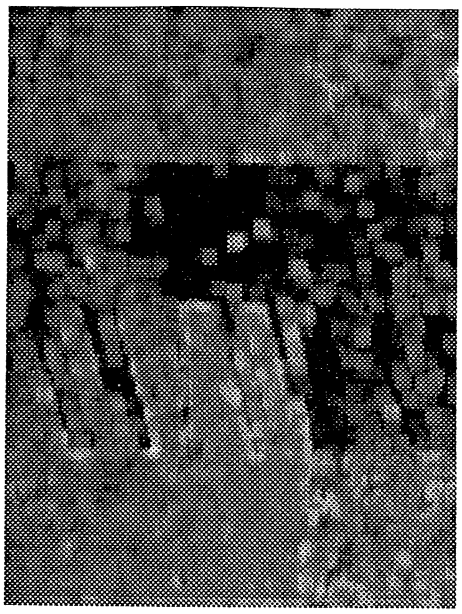

Figure 20: *Cluster prominence feature (GLCM). NIR.*

From Figure 23 we can see how the mean value of the entropy feature changes from sample to sample in quite different ways for the three illumination angles. None of the three seem to give a picture of the desired sample properties. One could say that the values for the high illumination angle give an inverted picture of the porosity and the quartz fraction values.

For the ASM feature (not shown here), the mean values vary in a similar manner, though in directions opposite to the changes in entropy. It does not seem to give direct information about the desired properties.

The last one of the four features used by Haralick for classifiaction of sandstone, is correlation. From a visual inspection of the feature images, it seemed that the feature might separate the samples well. In Figure 24 the mean values with oblique illumination only are shown. Here we see that the low illumination reflects the correct ordering of porosity and quartz fractions for all the samples. In figure 25, we see the same with additional diffuse illumination. In these two pictures the correct ordering of porosity and quartz is given in all illumination cases for sample 1,2 and 4, while the values for sample 3 mostly are too high to reflect the correct ordering.

3.5 Texture from region statistics

Figures 26 and 27 show the average area size and the standard deviation of the area size for each of the four texture types. As can be seen in Figure 35, the area sizes for sample number three is influenced by the lineaments within the sample. If we discard sampel

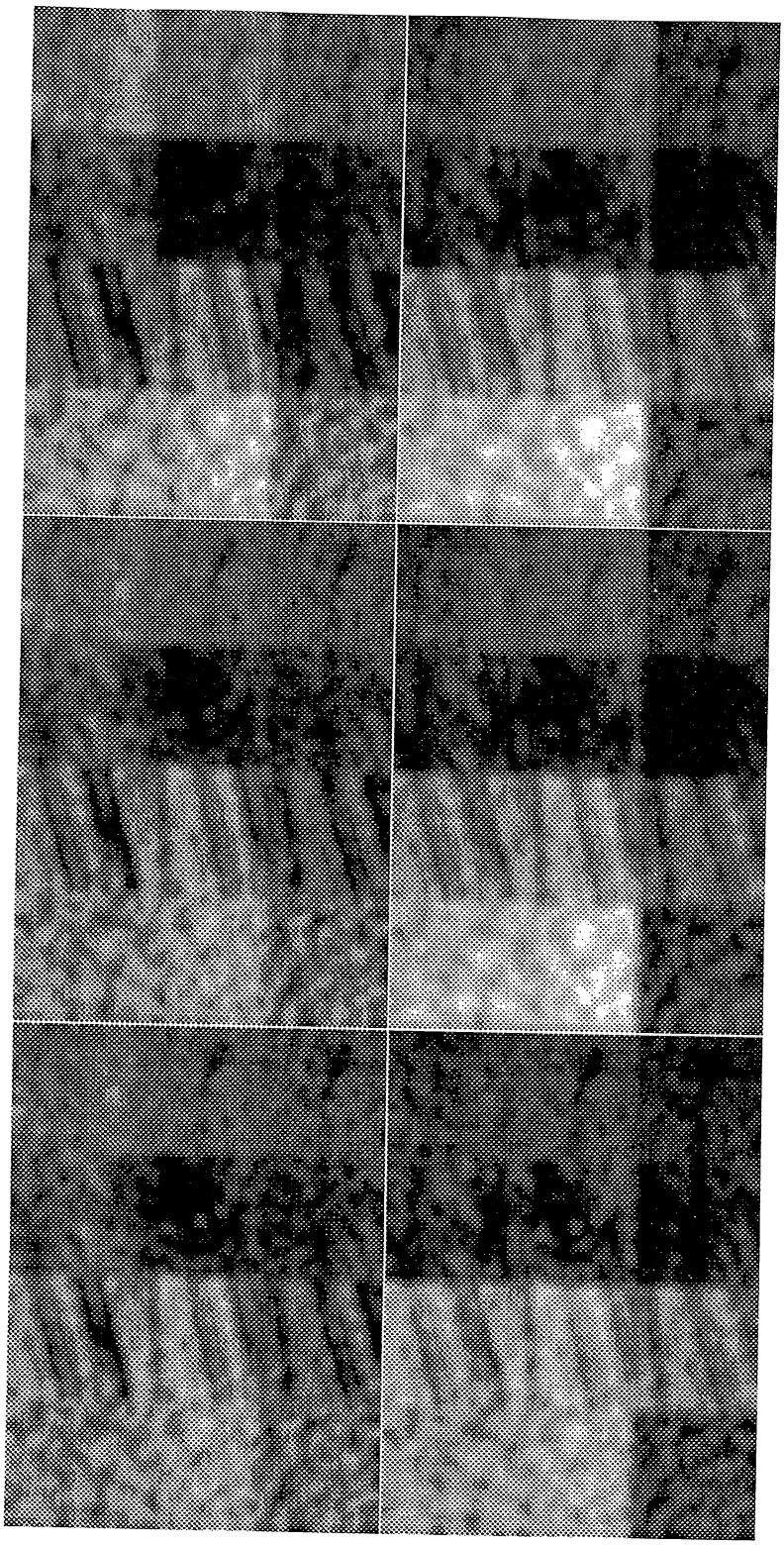

Figure 21: *Correlation feature with all frequency bands and types of illumination. Row 1, NIR; row 2, red; row 3, green; left column, oblique illumination; right column, additional diffuse illumination.*

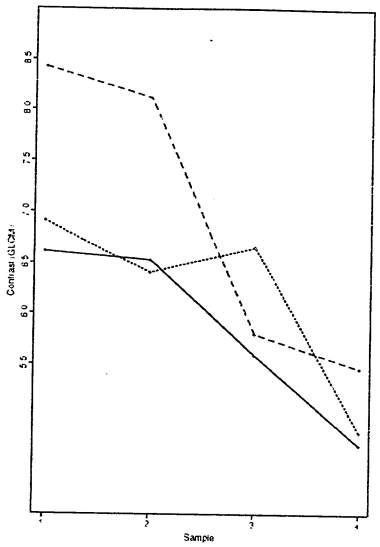

Figure 22: *Mean values of contrast feature (GLCM). NIR.*

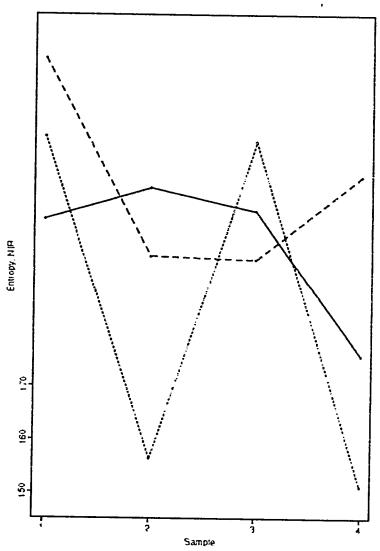

Figure 23: *Mean values of entropy feature (GLCM). NIR.*

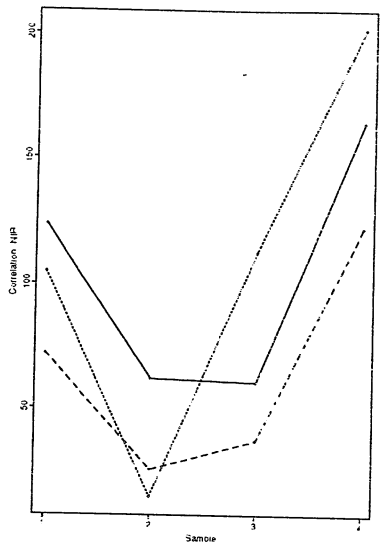

Figure 24: *Mean values of correlation feature (GLCM). NIR.*

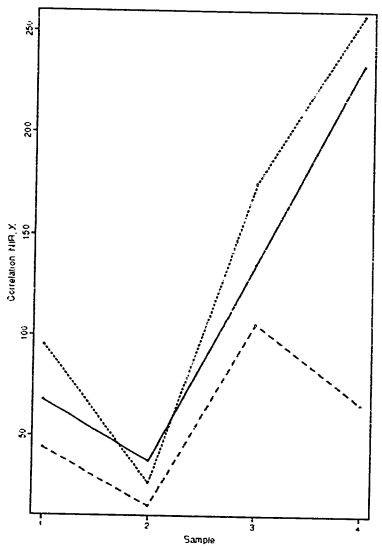

Figure 25: *Mean values of correlation feature (GLCM). NIR. Additional diffuse illumination.*

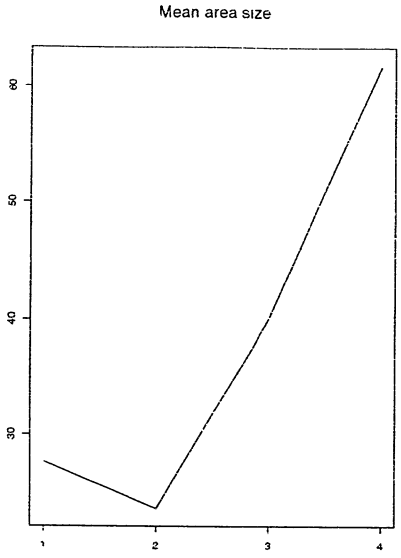

Figure 26: *Average area size for the four texture types.*

number three, then the mean area size and standard deviation seem to be related to the horisontal porosity and the quartz measurements.

3.6 The SAR model textural features

Of the five texture parameters of the SAR model, only the variance σ^2 and the mean μ_x provided any discriminative information with respect to the different stone textures. The resulting variance image is given in Figure 28, and the mean image in Figure 29. The mean image seems to indicate a correlation between the horizontal porosity and the quartz values. Our experience from the use of this model for other texture classification tasks is that the variance parameter improves the discrimination somewhat when used in combination with the mean parameter. In other texture applications involving the SAR model, we also found discriminative information in the θ parameters. However, it is not at this point clear if the differences in mean values for the different samples is a robust feature for classification, or if other lighting conditions may produce contradictory results.

3.7 Gabor filters

Due to the isotropic nature of the sandstone samples, orientation-specific filters were not included in the filter bank. Following the directions given by Jain and Farrakhnia [6], a filter bank of four filters with different frequencies were used (the maximum number of different frequencies depends on the image dimensions). The feature images corresponding

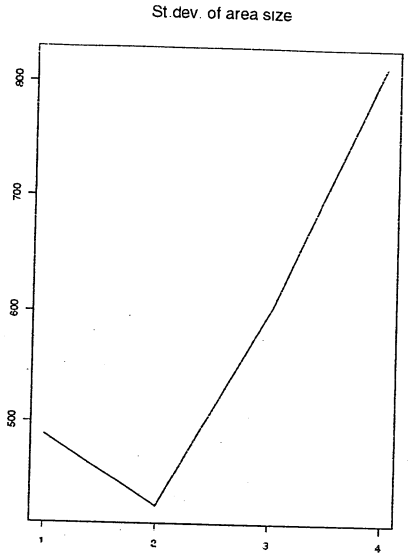

Figure 27: *Standard deviation of the area sizes for the four texture types.*

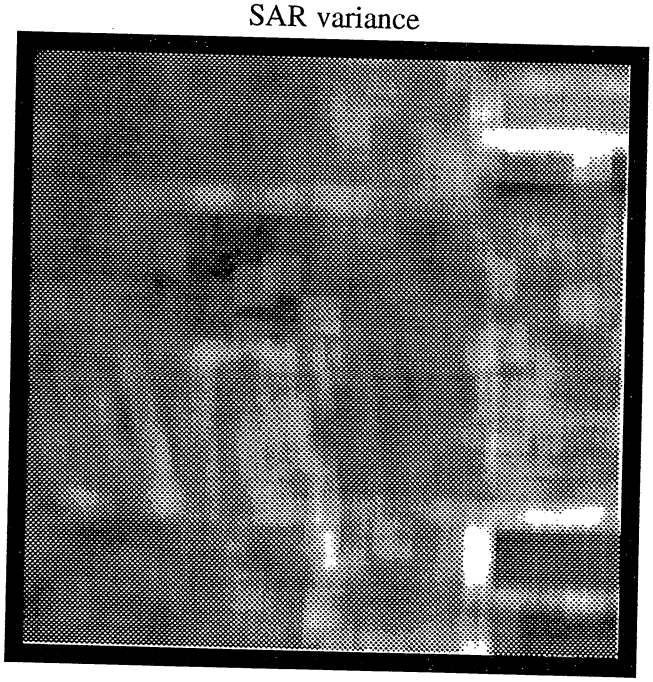

Figure 28: *SAR variance texture image.*

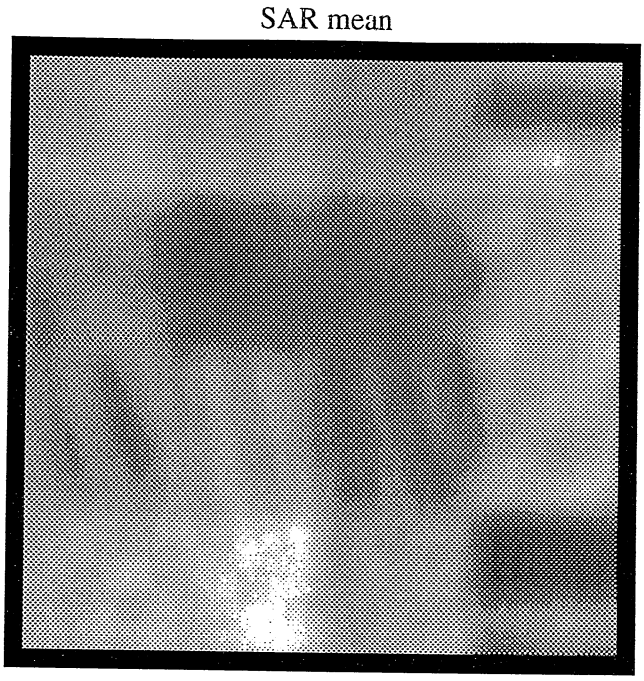

Figure 29: *SAR mean texture image.*

to the two highest frequencies are given in Figures 30 and 31. Only in the highest frequency image can certain differences among different samples be seen, but the discrimination of the samples is fairly low. From this limited study, we conclude that Gabor filters are not suited for texture classification of sandstone.

3.8 Texture measures computed from local statistics

Calculations have been done for some textural features based on local statistics for the near infrared band and without diffuse illumination. The following features have been treated:

- Power-to-mean ratio
- Skewness
- Curtosis
- Contrast
- Homogeneity
- LIT-SNN

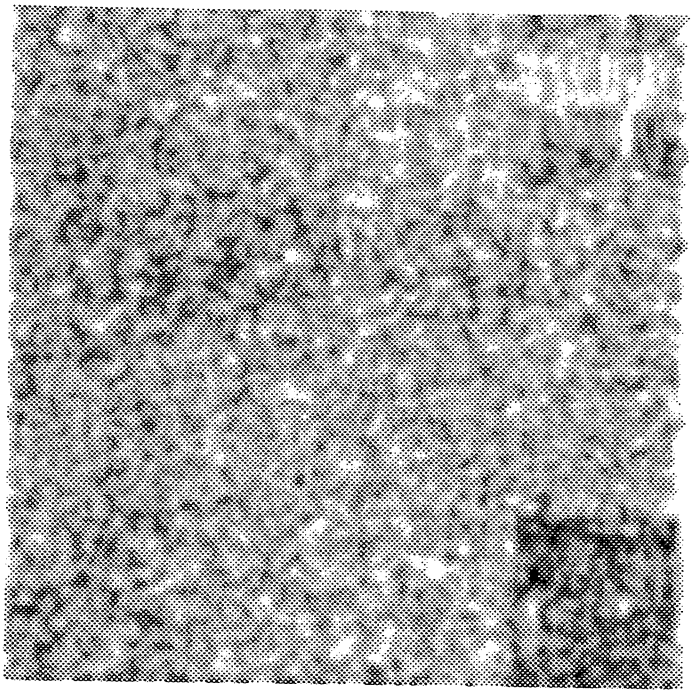

Figure 30: *Gabor texture image, feature 1.*

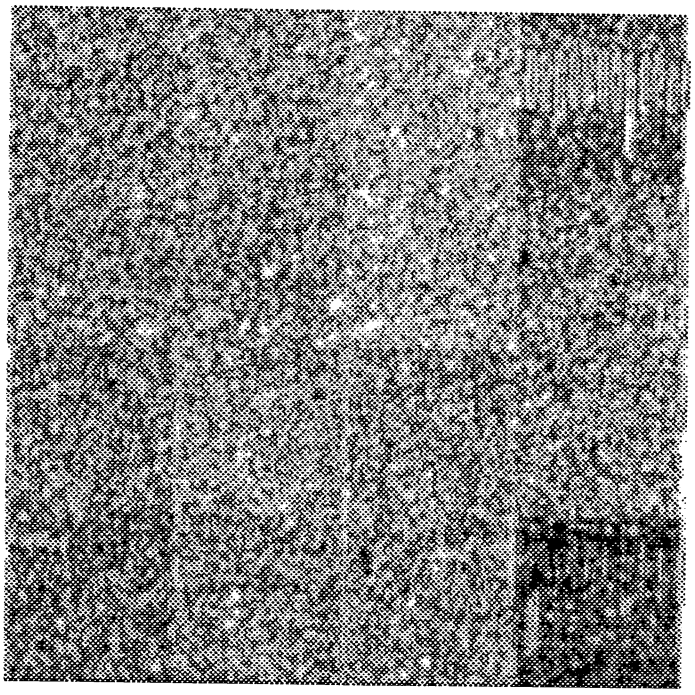

Figure 31: *Gabor texture image, feature 2.*

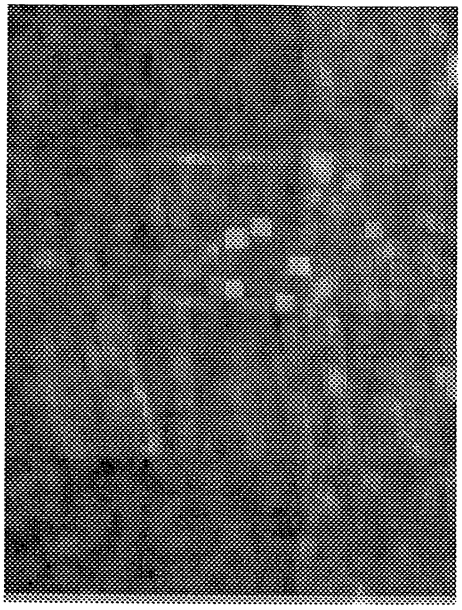

Figure 32: *Power to mean ratio feature. NIR.*

The computed feature images are shown in Figures 32 to 38. By visual inspection, the contrast feature image was found interesting. The mean values were calculated and are shown in Figure 36. This feature may reflect something about the interesting properties. With medium illumination the values show the correct ordering (inverted) of the samples according to porosity and quartz fraction.

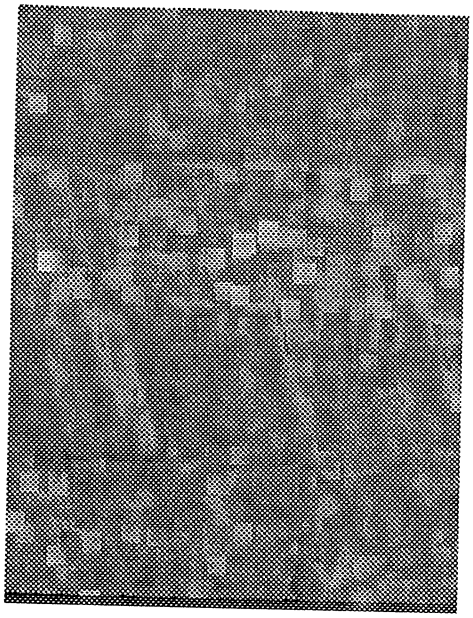

Figure 33: *Skewness feature. NIR.*

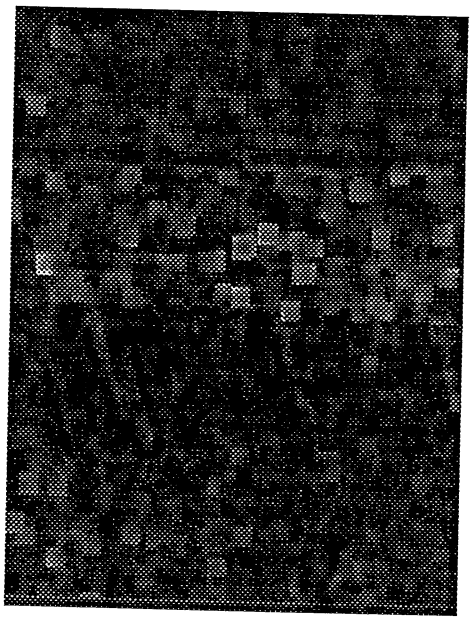

Figure 34: *Curtosis feature. NIR.*

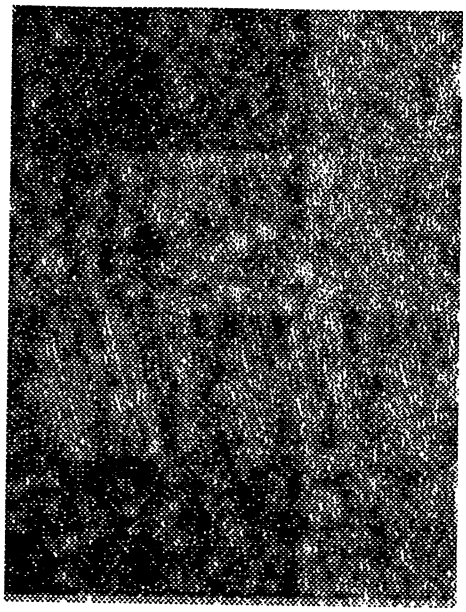

Figure 35: *Contrast feature. NIR.*

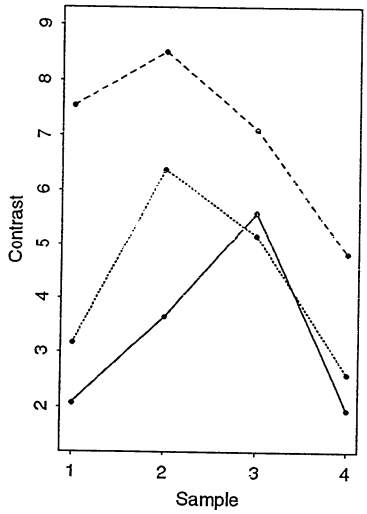

Figure 36: *Mean values of contrast feature. NIR.*

Figure 37: *Homogeneity feature. NIR.*

Figure 38: *LIT-SNN feature. NIR.*

4 Discussion and conclusions

A literature search indicates that very little is published on sandstone characterization using textural features. One of the few relevant publications is Haralick et al. [5] from 1973. They performed an experiment where sandstone facies were classified from the mean and variance of four different textural features. These were Angular Second Moment (ASM), Contrast, Correlation and Entropy. Class statistics were established from a training set of 143 of 5 different types of sandstone. A set of 100 new samples were classified, giving 89% correct classification.

The experiment by Haralick et al. indicates that sandstone characterization based on texture features should be possible to at least some degree. However, it is not known whether the facies samples applied in their experiment are representative for the sandstone facies used in our experiment.

A major disadvantage of our experiment is obviously the small test data set. With only one sample of each sandstone facies, no absolute conclusions can be drawn with respect to the discrimination ability of the textural features for the different facies. The results may be biased by to us unknown factors. The following conclusions must therefore be interpreted with respect to this.

The experiments indicate some relationships between the given sandstone characteristics and (1) gray-level value in the different spectral bands and (2) some of the textural features. Of the four sandstone facies parameters grain size, porosity, and contents of quartz and feldspar, we found indications of correlations between porosity and contents of quartz, and some of the textural features. Indications of correlations were found between gray level (especially in NIR) and for the textural features GLCM Correlation, SAR texture features, Contrast, and Homogeneity. Other textural features seem to have some discriminative properties, but at least they cannot be used separately.

Before work on further adaptation or development of textural operators is initiated, we strongly recommend that a test data set of a few hundred samples are compiled. The most promising textural features from this experiment should be applied on the new data set and tested by statistical classification methods. From these results, it should be possible to determine very accurately how high discrimination which can be expected with these textural features. If the experiment shows that it is necessary to improve the classification accuracy, the experiment may also indicate important properties which a more suited textural operator should show.

References

[1] F. Albregtsen, "Detection of Cancer by 2-D Texture Analysis of Liver Cell Nuclei", Presented at the NORSIG conference, Norway October 25-26, 1990.

[2] R. Chellappa and R. L. Kashyap, "Digital Image Restoration Using Spatial Interaction Models", *IEEE Trans. Acoust., Speech, Signal Processing*, vol. 30, pp. 461-472, 1982.

[3] R.W. Conners, M.M. Trivedi and C.A. Harlow, "Segmentation of a High-Resolution Urban Scene Using Texture Operators", *Computer Vision, Graphics, and Image Processing*, vol. 25, pp. 273-310, 1984.

[4] R. T. Frankot and R. Chellappa, "Lognormal Random-Field Models and Their Applications to Radar Image Synthesis", *IEEE Trans. Geosc. Remote Sensing*, vol. 25, pp. 195-206, 1987.

[5] R. Haralick, K. Shanmugam and I. Dinstein, "Textural Features for Image Classification", *IEEE Transactions on Systems, Man, and Cybernetics*, vol. SMC-3, No. 6, p. 610-621, November 1973.

[6] A. K. Jain and F. Farrokhnia, "Unsupervised Texture Segmentation Using Gabor Filters", *Pattern Recognition*, vol. 24, pp. 1167-1186, 1991.

[7] R. L. Kashyap and R. Chellappa, "Estimation and Choice of Neighbors in Spatial-Interaction Models of Images", *IEEE Trans. Inform. Theory*, vol. 29, pp. 60-72, 1983.

[8] J. D. Lyden, B. A. Burns, and A. L. Maffett, "Characterization of Sea Ice Types Using Synthetic Aperture Radar", *IEEE Trans. Geosc. Remote Sensing*, vol. 22, 1984.

[9] H. Skriver and P. Gudmansen, "Study on the Use and Characteristics of SAR for Sea Ice and Polar Ice Applications", Electromagnetic Institute, Techichal University of Denmark, R 307, Final Report, ESA Contract No. 5442/83/D/IM(SC), Denmark, June 1986.